

Lawrence Berkeley National Laboratory

Lawrence Berkeley National Laboratory

Title

Al₂O₃ Scale Development on Iron Aluminides

Permalink

<https://escholarship.org/uc/item/6cb7443m>

Authors

Zhang, Xiao-Feng
Thaidigsmann, Katja
Ager, Joel
et al.

Publication Date

2005-11-10

Peer reviewed

Al₂O₃ Scale Development on Iron Aluminides

X.F. Zhang¹, K. Thaidigsmann², J. Ager¹, and P.Y. Hou^{1*}

¹Materials Sciences Division
Lawrence Berkeley National Laboratory, Berkeley, CA 94720

²University for Applied Science
Department Material Sciences and Surface Technology
Beethovenstrasse 1, 73430 Aalen, Germany

*Correspondence should be addressed to this author

ABSTRACT

The structure and phase of the Al_2O_3 scale that forms on an Fe_3Al -based alloy (Fe-28Al-5Cr (at %)) was investigated by transmission electron microscopy (TEM) and photoluminescence spectroscopy (PL). Oxidation was performed at 900°C and 1000°C for up to 190 min. TEM revealed that single-layer scales were formed after short oxidation times. Electron diffraction was used to show that the scales are composed of nanoscale crystallites of the θ , γ , and α phases of alumina. Band-like structure was observed extending along three 120° -separated directions within the surface plane. Textured θ and γ grains were the main components of the bands, while mixed α and transient phases were found between the bands. Extended oxidation produced a double-layered scale structure, with a continuous α layer at the scale/alloy interface, and a γ/θ layer at the gas surface. The mechanism for the formation of Al_2O_3 scales on iron aluminide alloys is discussed and compared to that for nickel aluminide alloys.

Key Words: Intermetallic alloys, Microstructure, TEM.

I. INTRODUCTION

A slow growing, adherent and chemically stable oxide layer is an essential component of any metal alloy that is designed for high-temperature operation. For most Al-containing high-temperature alloys and coatings, including for example Ni-based superalloys, Ni or Fe aluminides and FeCrAl alloys, this layer is composed of Al_2O_3 . The aluminides, being high temperature intermetallics, have been vigorously pursued since the early 1950s for aerospace and power-generation industries due to their high melting points and low densities. Although their brittleness, especially at ambient temperatures, and low strengths at high temperatures have greatly hindered their applicability, NiAl has been successfully used as an oxidation resistant coating, and Ni_3Al and Fe_3Al -based materials are being commercialized for applications such as industrial heat treatment equipment and hot gas filters [1]. The development and evolution of Al_2O_3 scales on NiAl has been studied extensively by TEM, but there are comparatively fewer studies of this process for FeAl. Past works on the scale development on NiAl and FeAl are first summarized below.

On β -NiAl, Doychak et al [2] studied the oxidation of (001), (012), (011) and (111) single crystals containing 0.1wt% Zr using plan-view TEM specimens. The major oxide phase was identified as θ - Al_2O_3 within 10 hrs at 800°C and 0.1 hrs at 1100°C , although some δ phase may be present between 0.1-1 hr at 800°C . On all alloy orientations, the scale formed epitaxially, whereas the degree of preferred orientation decreased with oxidation time. The same alloy was also studied by Rybicki and Smialek using X-ray diffraction [3] and found the transition alumina to be θ - Al_2O_3 , which later transformed to α - Al_2O_3 . The time at which this transformation took place was shorter at higher oxidation temperature. Later, Yang et al [4], using conventional and high resolution cross-sectional TEM, found on (001)NiAl with 0.01 wt% Y, after 950°C in air for 6 minutes, epitaxially grown γ - Al_2O_3 with the Bain relationship: $(001)_{\text{NiAl}} // (001)_{\gamma\text{-Al}_2\text{O}_3}$ and $[100]_{\text{NiAl}} // [110]_{\gamma\text{-Al}_2\text{O}_3}$. The γ - Al_2O_3 had a platelet type morphology and the oxide/alloy interface was coherent. With further oxidation, randomly oriented α - Al_2O_3 grains nucleated at the scale/alloy interface [5]. Similar TEM studies have not been performed on FeAl alloys. Smialek et al

[6] studied the oxidation behavior of Fe-40Al doped with Hf, Hf+B or Zr+B between 900-1100°C and found, using XRD, the Al₂O₃ scale to be a mixture of θ and α -Al₂O₃.

For γ' -Ni₃Al, an external layer of Ni-rich oxide was always detected, beneath which is the Al₂O₃ layer. Like the Al₂O₃ that forms on β -NiAl, this Al₂O₃ layer may have started as the γ form, and then later transformed to the more stable α phase. Kuenzly and Douglass [7] studied oxidation of polycrystalline γ' -Ni₃Al, and found by XRD and SEM that the scale formed at 900°C consisted of an outer layer of NiO, an intermediate layer of NiAl₂O₄ and an inner layer of α -Al₂O₃. At 1200°C, Doychak and Rühle [8] found by cross-sectional TEM a duplex scale of NiAl₂O₄ and α -Al₂O₃ on polycrystalline γ' -Ni₃Al+Zr. Shumann et al [9] studied the oxide development on (001) γ' -Ni₃Al at 950°C; initially (after 1 min), an external layer of NiO and an internal oxidation zone of γ -Al₂O₃ formed, where the internal oxide precipitates had a cube-on-cube orientation relationship with the alloy: (001)[110]_{Ni} // (001)[110] _{γ -Al₂O₃}. After 6 min, a complete γ -Al₂O₃ layer formed at the internal oxidation front, which maintained the same cube-on-cube relationship with the alloy. Eventually, the entire internal oxidation zone was oxidized and the scale consisted of an outermost layer of NiO, an intermediate layer of NiAl₂O₄ and an inner layer of Al₂O₃. After 50 hrs, most of the Al₂O₃ was still γ -Al₂O₃, but α -Al₂O₃ was found to form at the scale/alloy interface, as well as within the γ matrix.

Unlike Ni₃Al, Fe₃Al alloys do not seem to develop a noticeable Fe-rich surface layer [10]. Rensch et al [11] studied the initial stage scale development as a function of temperature in Fe₃Al-based alloy (Fe-28Al-5Cr, at%) using Raman and photoluminescence (PL) spectroscopy. The first detected oxide was Fe₂O₃, whose intensity increased from 500-700°C, then dropped to zero with continued oxidation at higher temperatures. α -Al₂O₃ was detected as early as 750°C and its intensity quickly increased with longer times at higher temperatures. After 900°C, Fe₂O₃ was no longer detected. The authors suggested that Fe₂O₃, having the same corundum structure as α -Al₂O₃, served as templates that facilitated the nucleation and growth of the α phase at a temperature below which this transition happens in the bulk (1000°C). It was also suggested that Cr₂O₃ can also serve as a template for low temperature α -Al₂O₃ growth on FeCrAl type alloys [11], similar to that

proposed by Hagel [12]. A recent XRD study of the same Fe₃Al-based alloy oxidized at 900 or 1000°C in oxygen found the first developed oxide to be θ -Al₂O₃ [13]; α -Al₂O₃ was detected after 10 minutes at 1000°C and 1 hr after 900°C

In summary, only Al₂O₃ is formed on β -NiAl at elevated temperatures (>800°C). The first formed alumina is either the metastable γ or the θ phase, or a combination of the two. The oxide at this stage has a cube-on-cube orientation relationship with the alloy and the interface may be coherent. With further oxidation, randomly oriented α -Al₂O₃ nucleates at the scale/alloy interface and they form an incoherent interface with the alloy. These nuclei eventually develop into a complete α -Al₂O₃ layer above the alloy, and initially formed γ and/or θ alumina transform to the α -Al₂O₃ phase with time. The transformation is faster at higher temperatures. NiO and/or NiAl₂O₄ always develop above the Al₂O₃ layer on Ni₃Al, but much less Fe-containing oxides seem to form on Fe₃Al. Similar alumina phase transformation from θ to α seem to also occur on β -FeAl.

In contrast to the detailed knowledge of the evolution of the alumina scales on β -NiAl and Ni₃Al, less is known about the early stages of oxide formation on Fe₃Al alloys, particularly with respect to the transformation of the metastable γ and/or θ phase to the most stable α -Al₂O₃ phase with time. Here we present a detailed TEM study of scale development on Fe₃Al and develop a full picture of its initial oxidation process between 900 and 1000°C. The goal is to compare this process with that found on Ni-based alloys, in order to better understand the role of different substrate components.

II. EXPERIMENTAL METHODS

The major alloy studied was developed and made at Oak Ridge National Laboratory with a nominal composition of Fe-28Al-5Cr (in atomic %), where the Cr is added to the Fe₃Al alloy to increase its ductility [14]. Actual composition determined by inductively coupled plasma-emission spectroscopy confirmed these values, with 27.88 at% Al and 4.98 at% Cr. The major impurity was Si, at a level of 0.03 at%, and GDMS (glow discharge

mass spectrometry) analysis found 34 ppma S, 48 ppma N and 68 ppma O. The alloy was prepared by arc melting and casting, followed by hot rolling to a final thickness of 1.4 mm. A Fe-28at%Al alloy, without the Cr addition, and a Ni-50at%Al alloy were also investigated under photoluminescence spectroscopy for comparison. These alloys were prepared similarly by arc melting, casting and annealing. Specimens were cut from the annealed ingot.

For plan-view TEM samples, 10×10 mm pieces were first cut from the rolled sheet and then ground to a thickness of 0.2 mm. For cross-sectional specimens, the thinned pieces were further cut into $2 \times 10 \times 0.2$ mm strips. Before oxidation, one side of each prepared specimen was polished using diamond paste to a 1 μm finish, followed by ultrasonically cleaning in acetone.

Oxidation runs were performed in a horizontal furnace pre-heated to the oxidation temperature, 900 or 1000°C, with a steady flow of oxygen. Each specimen was placed in an alumina boat with a thermocouple touching its back to directly monitor the specimen temperature. At the start of an oxidation run, the alumina boat was slowly pushed into the hot zone of the furnace. Oxidation times varied from 4.5, 35 to 190 minutes at 900°C and 3 to 10 minutes at 1000°C. The final specimen temperature of the 4.5 min and the 3 min samples was only $\sim 850^\circ\text{C}$ and 910°C respectively. Heating to within three degrees of the desired oxidation temperature usually takes 8-10 minutes.

Plan-view TEM samples were prepared by punching 3 mm diameter discs out of the oxidized thin specimen. Each disc was then dimpled and ion-milled from the alloy side. For cross-sectional TEM samples, the technique similar to that developed by Tinker and Labun [15] is used, where two oxidized strips were glued together with oxidized sides face to face using M-Bond 610 adhesive. The sandwich assembly was then embedded with liquid epoxy resin into a 3 mm diameter support tube. Using a slow-cutting diamond saw, 3 mm diameter circular slices with a $250\mu\text{m}$ thickness were cut from the tube and examined under an optical microscope. Those that were flat with a uniform, adherent and thin glue layer were grounded and ion-milled till electron transparency. TEM observations were carried out using a 200kV field-emission gun Philips CM200 microscope with an

energy-dispersive X-ray spectroscopy (EDS) for chemical analysis. Electron diffraction was used to identify the oxide phases.

Photoluminescence spectroscopy was used to detect α - Al_2O_3 and θ - Al_2O_3 via the Cr^{3+} emission line. The 488 nm line of an argon ion laser was used for excitation and a 0.75 m double spectrometer was used for detection.

III. RESULTS

As expected from previous reports [11], the Fe_3Al -based alloy did not develop significant amounts of Fe-rich oxides upon oxidation at 900 or 1000°C. Fig. 1 shows Auger electron spectroscopy (AES) depth profiles through the thin surface films formed on specimens oxidized in a 1000°C furnace after 3 and 10 minutes, where the specimen temperature reached 910°C after 3 min, and 1000°C after 10 min. Even after 3 minutes, with the specimen continually being heated, the scale consisted mainly of Al and O. More Fe was found in this initial scale, as compared between the 3 and 10 minute profiles, but Fe was incorporated within a well-developed Al_2O_3 layer. After 10 minutes, only very small amounts of Fe, <2 at%, was detected on the surface of the Al_2O_3 scales. The presence of 5 at% Cr in the current alloy does not seem to contribute to the scale development, because an Fe-28at%Al alloy, without the Cr addition, also developed similar Al_2O_3 layers when oxidized between 900-1100°C [16].

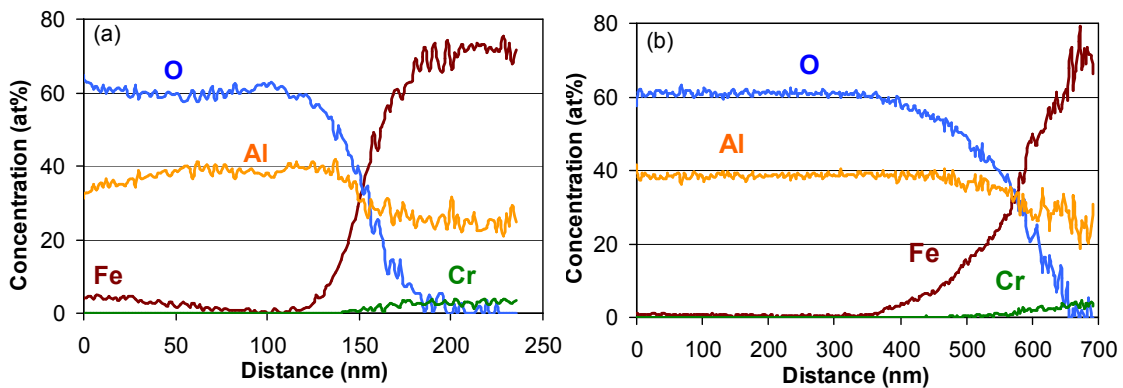


Fig. 1: Auger electron spectroscopy depth profiles of scales formed on a Fe_3Al -based Fe-28Al-5Cr alloy after (a), 3 min and (b), 10 min in a 1000°C furnace.

A cross-sectional TEM micrograph of the scale formed at 900°C for 4.5 minutes is shown in Fig. 2a. A continuous film 50 to 85 nm thick consisting mainly of Al and O was observed. The randomly oriented nanoscale crystallites in the scale made phase identification difficult. EDS analyses across the film showed Fe enrichment toward the film surface up to 11.5wt%, similar to that found by AES (Fig. 1), and Cr was slightly enriched, 3.5wt%, in the Al₂O₃ near the film/alloy interface, Fig. 2b. The interface between the film and the substrate was smooth and abrupt, without secondary phases, nor was sulfur detected, similar to previous results using AES that showed the interface at this stage is impurity free [13]. Similar compositions and structures were observed on specimens oxidized at 1000°C for 3 minutes. In Fig. 2, the film is seen to be composed of

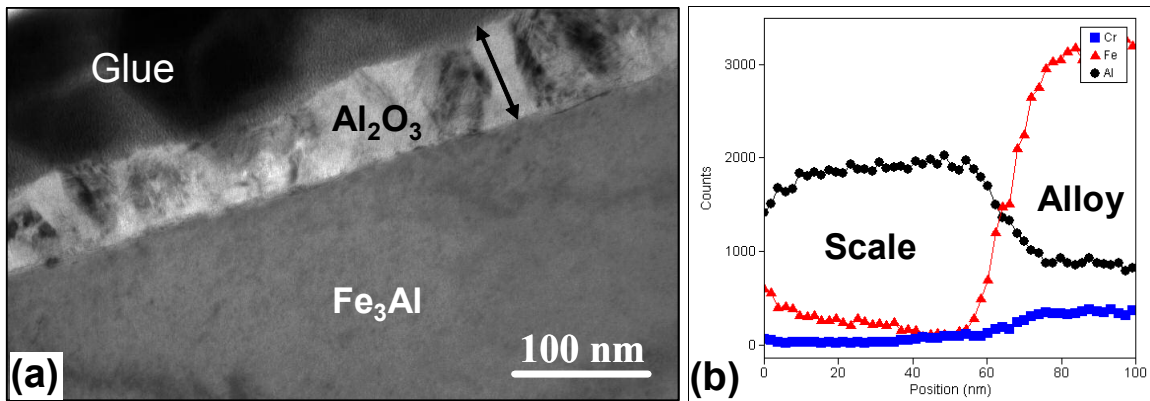


Fig. 2: (a), Cross-sectional morphology of Al₂O₃ scale oxidized on a Fe₃Al alloy at 900°C for 4.5 min. The glue layer was applied during TEM sample preparation. (b), EDS line scan across the thickness of Al₂O₃ scale.

crystalline grains with sizes between 2 and 70 nm. Pores with 5 to 10 nm diameter were observed in the middle of the film although they are not apparent in Fig. 2. Some through-thickness columnar grains are seen; an example is marked by arrows on the micrograph. Between these larger grains are much smaller crystallites. Fig. 3 shows two of them, 15 to 20 nm in diameter, which were observed under high-resolution TEM. Areas surrounding

these two grains were not correctly oriented under the beam, indicating no preferred orientation of all oxide grains in the fine-grained regions.

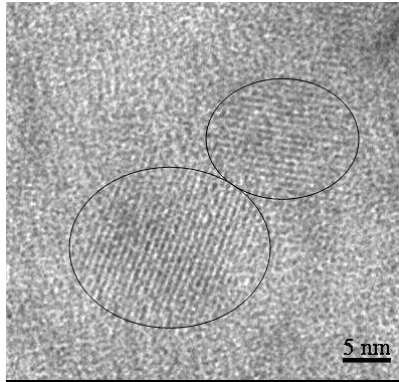


Fig. 3: High-resolution electron micrograph showing two nanoscale grains in the cross-sectional Al₂O₃ scale oxidized at 900°C for 4.5 min. Lattice fringes within grains are recognized.

Extending the oxidization time to 35 min at 900°C thickened the Al₂O₃ scale, but the scale remained single layered, consisting mainly of Al and O, with detectable Fe. Electron diffraction identified θ - and γ -Al₂O₃ phases. In another sample oxidized at 1000°C for 10 min, α -Al₂O₃ grains were seen to nucleate at the scale/alloy interface (Fig. 4) and started to form a complete layer above the alloy, similar in behavior to the specimen oxidized at 900°C for 190 min. Sub-micron sized voids were sometimes observed at the interface, extending into the alloy.

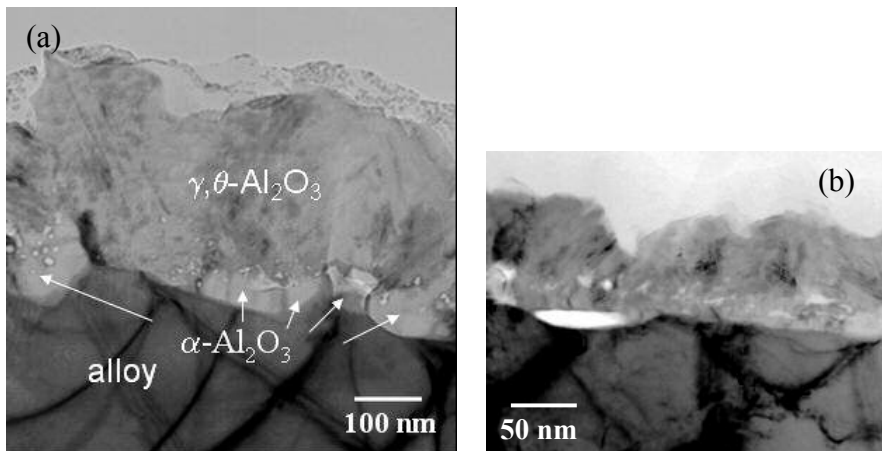


Fig. 4: Cross-sectional TEM images of an alloy oxidized at 1000°C for 10 min. (a) α -Al₂O₃ grains nucleated at the scale/alloy interface as indicated by arrows. Small voids are seen in the scale between the alpha and transition alumina, and (b) large voids are sometimes detected at the scale/alloy interface.

Plan-view samples were studied, focusing on phase constitutions. Typical plan-view morphologies of scales formed at 900°C for 4.5 min, 35 min and 190 min with corresponding diffraction patterns are presented in Figs. 5-7, respectively. The scales consisted of polygonal grains whose size increased with oxidation time. Under higher magnifications (not shown here), pores of 5-20 nm in diameter were found randomly distributed in the oxide films. The most striking feature in Figs. 5 and 6, but not in Fig. 7, is the appearance of dark-contrast bands that are roughly along three, 120°-apart directions, whose lengths range from 50 to 200 nm, and widths from 10 to 40 nm. The total area fraction of these bands was 68% in the 4.5 min scale, 42% after 35 min oxidation, and 0% after 190 min. The area fraction of each set among the three sets of bands is always similar to the other two. EDS analysis confirmed the same Al₂O₃ composition with minor Fe content in both the band areas and the areas in-between.

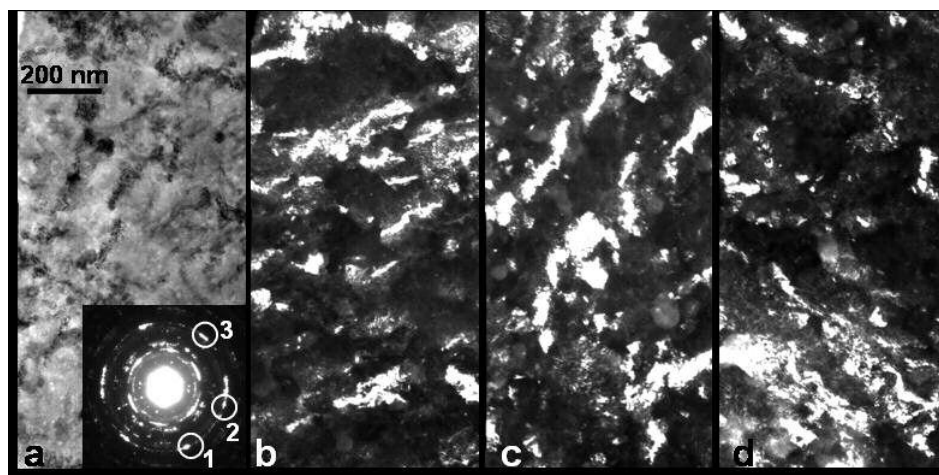


Fig. 5: (a), Bright-field plan-view TEM image taken from the Al₂O₃ scale oxidized on a Fe₃Al alloy at 900°C for 4.5 min. Corresponding electron diffraction ring pattern is inserted, in which strong reflection loci used for dark-field imaging are circled and marked with 1, 2, and 3. (b), (c), (d), Dark-field images using diffraction spots 1, 2, and 3, respectively, marked in the inset of (a).

For the 4.5 and 35 min scales, diffraction loci with stronger than average intensities and a roughly 3- or 6-fold symmetric arrangement about the central spot are clearly seen in electron diffraction patterns (Figs. 5a and 6b). A close correlation exists between the strong loci in the diffraction patterns and the three sets of bands in the micrographs. Dark-field images produced by diffraction loci marked with 1, 2, and 3 in the inset of Fig. 5a are

shown in Figs. 5b, c, and d, respectively. In each dark-field image, the excited bands are in bright contrast. These results indicate that the grains in the bands were not randomly oriented but had certain preferred orientations.

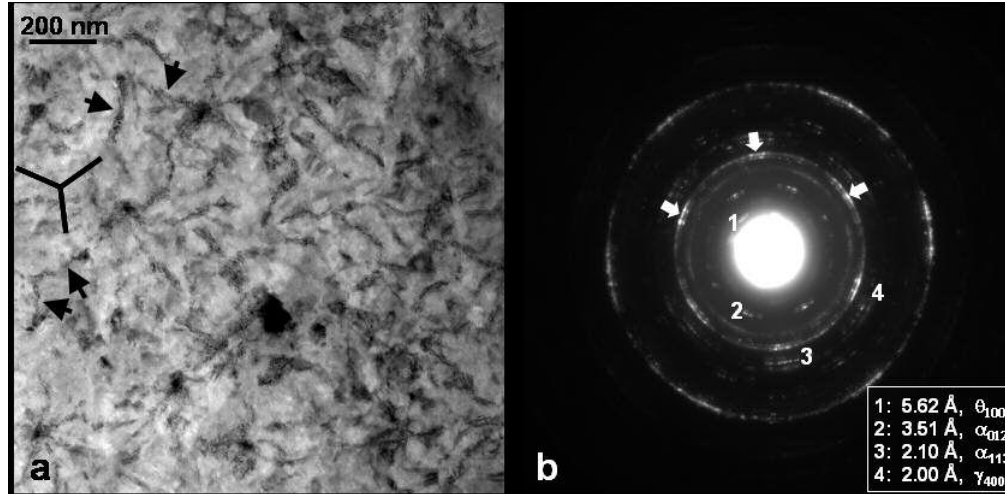


Fig. 6: (a), Plan-view morphology of Al_2O_3 scale oxidized on a Fe_3Al alloy at 900°C for 35 min. Arrows indicate dark-contrast bands which are along three directions as marked by lines. (b), Electron diffraction ring pattern taken with a $4.4\ \mu\text{m}$ diameter selected-area aperture. d-spacing values and the Al_2O_3 polymorphs corresponding to the rings marked by 1, 2, 3, and 4, respectively, are listed in an inserted table. Arrows indicate strongly excited diffraction loci on a diffraction ring.

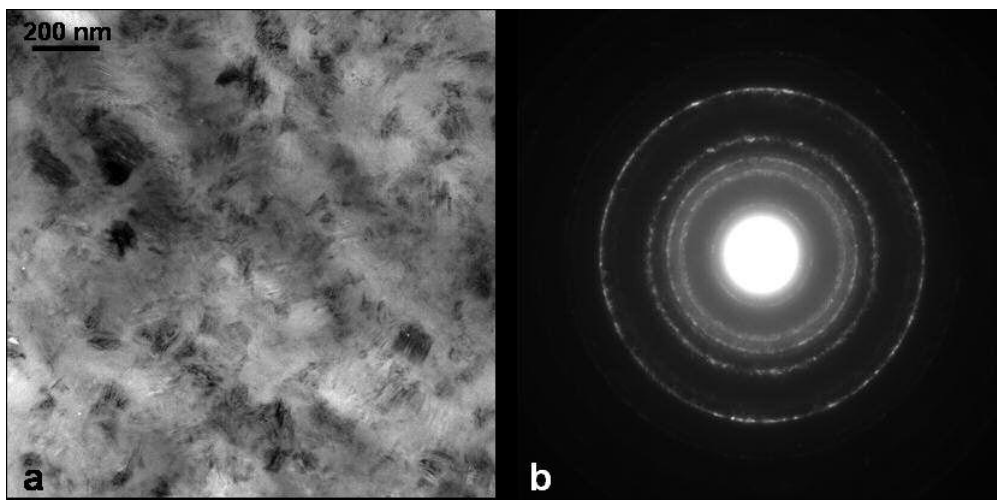


Fig. 7: (a), Plan-view morphology of the Al_2O_3 scale oxidized on a Fe_3Al alloy at 900°C for 190 min. The band structure observed in the 4.5 and 35 min oxidation films disappeared. (b), Corresponding electron diffraction ring pattern taken from a $4.4\ \mu\text{m}$ diameter area.

While the d-spacing of most diffraction rings in electron diffraction patterns could correspond to either the α -, θ - or γ - Al_2O_3 phase, some rings are unique representatives of specific Al_2O_3 polymorphs. The diffraction pattern in Fig. 6b was taken from a 4.4 μm diameter area where exposure time was adjusted to reveal the innermost rings. The ring marked by 1 corresponds to θ - Al_2O_3 only, and the two rings marked by 2 and 3 are from the α -phase. These d-spacing values and the corresponding phases with (hkl) indices are listed in the inset of Fig. 6b. From the electron diffraction ring patterns, it was concluded that both the 4.5 min and 35 min oxidation films were composed of mainly θ - and α - Al_2O_3 phases. γ - Al_2O_3 also existed, but in less amount, as indicated by the d-spacing of Ring 4 in Fig. 6b and its intensity, and from ring patterns of pure γ - Al_2O_3 regions that will be shown later.

The strong intensity diffraction loci found for the 4.5 min and 35 min scales appeared only on specific diffraction rings, e.g. those indicated by arrows in Fig. 6b. Reducing the selected area to a 1.8 μm diameter made the 3- or 6-fold loci more prominent, Fig. 8a. The diffraction rings containing the loci could correspond to either θ -, γ -, or α - Al_2O_3 phase, making it difficult to distinguish which phases actually made the contribution. To clarify the phase, electron diffraction patterns were taken using a 0.2 μm selected-area aperture, small enough to include only the grains in a single band. Such a diffraction pattern is shown in Fig. 8b, where two sets of hexagonal patterns were seen superimposed on each other, with a fixed 30° angle in-plane rotation about the central axis. Each set of the diffraction spots shows single crystalline characteristic. Careful analysis concluded that the hexagons marked by dashed lines correspond to the γ - Al_2O_3 $[111]$ pattern, and the one marked by solid lines the $[\bar{1}01]$ θ - Al_2O_3 with a slight lattice deviation. Both sets of diffraction spots fit perfectly with the strong intensity loci in Fig. 8a. The fact that the diffraction pattern in Fig. 8b was frequently seen in both 4.5 and 35 min oxidation films implies a possible intergrowth of the two phases with fixed orientation relationships within the bands.

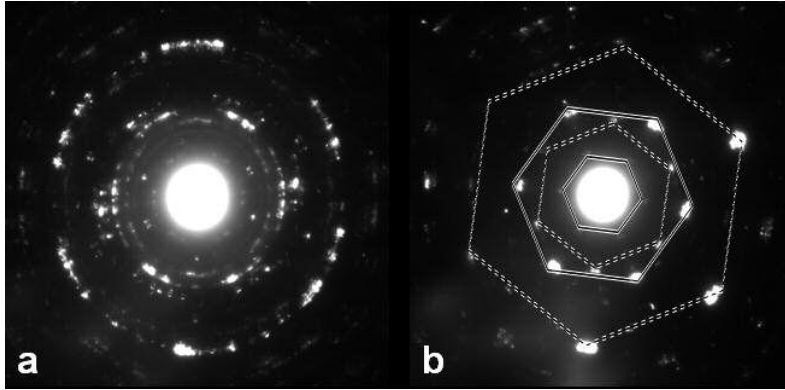


Fig. 8: (a), Selected-area electron diffraction pattern taken from Al₂O₃ scale oxidized on a Fe₃Al alloy at 900°C for 4.5 min. A 1.8 μm diameter selected-area aperture was used. Strongly excited diffraction loci with a 3- or 6-fold symmetric arrangement can be seen. (b), Electron diffraction pattern taken from a 0.2 μm diameter area within the single band as shown in Fig. 5a. Diffraction spots from θ -, and γ -Al₂O₃ phases are connected with solid and dashed lines, respectively.

Selected-area electron diffraction was also performed in the areas outside the bands, using the 0.2 μm diameter aperture. The scattered spots in the patterns matched either α -, θ -, or γ -Al₂O₃ phase, so the oxides outside the bands probably consisted of a mixture of the three polymorphs. Since larger area diffraction (Fig. 6b) shows γ as the least abundant phase in the overall scale and Fig. 8b identified the bands to consist of θ - and γ -Al₂O₃ grains, the areas between the bands must be richer in α - and θ -Al₂O₃.

In an area of the TEM foil where a portion of the alloy remained underneath the Al₂O₃ scale, plan-view electron diffraction ring patterns were taken, Fig. 9a. The strong intensity loci, which have been seen in the scales, appeared again in these ring patterns and are marked with arrows. The substrate was a single grain of the Fe₃Al type alloy viewed along the [001] direction, indices are marked, where subscript FA denotes the iron aluminide alloy. Orientation relationships between the textured film and the underlying substrate grain can be determined. Fig. 9b shows a simulated Fe₃Al [001] electron diffraction pattern superimposed with a simulated θ -Al₂O₃ [$\bar{1}01$] pattern. The $\theta(111)$ ring is marked by a dashed circle, on which strong loci are located (see the corresponding dashed-line circle in Fig. 9a). It can be seen that the simulated pattern in Fig. 9b indeed

represents the experimental pattern in Fig. 9a, except Fig. 9b contains only one set of the θ - Al_2O_3 $[\bar{1}01]$ pattern whereas Fig. 9a contains multiple sets with a rotation of up to 22° about the zone axis direction. In addition to the $\theta\{111\}$ reflections, $\gamma\{311\}$ reflections may also be part of the loci on the dashed-line circle. Fig. 9 and Fig. 8 suggest a probable orientation relationships between the textured θ/γ - Al_2O_3 bands and the substrate, e.g., $[001]_{\text{Fe}_3\text{Al}}//[\bar{1}01]_{\theta\text{-Al}_2\text{O}_3}//[111]_{\gamma\text{-Al}_2\text{O}_3}$, with in-plane rotation angles between 0 and 22° .

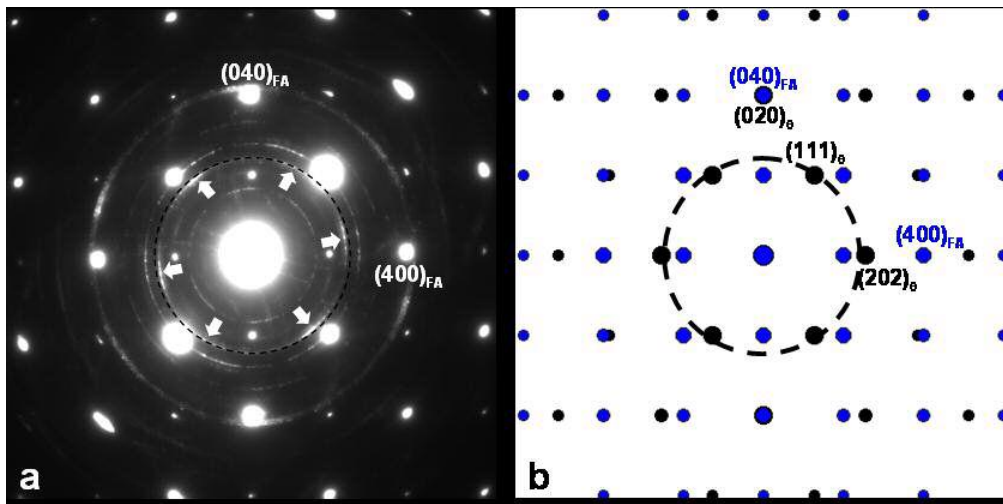


Fig. 9: (a), Electron diffraction pattern taken from Al_2O_3 scale oxidized on a Fe_3Al alloy at 900°C for 35 min. Diffraction spots from Fe_3Al substrate (denoted as FA) projected along the $[001]$ direction are indexed. Superimposed diffraction rings from Al_2O_3 scale are seen. Strongly excited, 3- or 6-fold symmetric loci are indicated by arrows. (b), Simulated Fe_3Al $[001]$ electron diffraction pattern is superimposed on a simulated θ - Al_2O_3 $[\bar{1}01]$ diffraction pattern. A dashed circle marks the $\theta(111)$ ring which matches the ring marked by the dashed circle in (a).

In contrast to the 4.5 and 35 min oxidation films, structure in the 190 min oxidation films looked quite different. Fig. 7a shows that the Al_2O_3 grains were considerably coarsened after this time; the grain size ranged from 60 to 250 nm. EDS revealed Al_2O_3 and a small amount of Fe in each grain, same as in the shorter time oxidation films. The band structures seen in shorter time oxidation have now disappeared. Surprisingly, all

characteristic α - Al_2O_3 rings also disappeared from the diffraction ring pattern shown in Fig. 7b, which matched well with γ/θ - Al_2O_3 . Similar ring patterns were obtained from 20 different regions, far from each other, in the same sample to verify the lack of the α -phase. Noticing that the plan-view samples were thinned from the substrate side and the final sample thickness for TEM was only a few tenths of the whole scale thickness in this case, it is possible that grinding and ion milling from the substrate side removed the α -phase layers that were present near the interface (similar to the structure shown in Fig. 4). It is therefore safe to conclude that at least near the top surface area, the major phases were γ and θ - Al_2O_3 .

Some areas of the 190 min specimen, about $70 \times 200 \mu\text{m}$ dimension, contained only needle-like grains as shown in Fig. 10a. The size of the needles is uniform, about 0.3-0.5 μm in length, and $\sim 0.1 \mu\text{m}$ in width. The ring pattern, shown in Fig. 10b, corresponds to pure γ - Al_2O_3 phase; this conclusion was also supported by selected-area electron diffraction patterns from individual needle grains, Fig. 10c and 10d, which provide unambiguous evidence for the γ - Al_2O_3 structure. Fig. 10b was used in this study as a reference pattern for γ - Al_2O_3 identification in analyzing the superimposed ring patterns such as that in Fig. 7b.

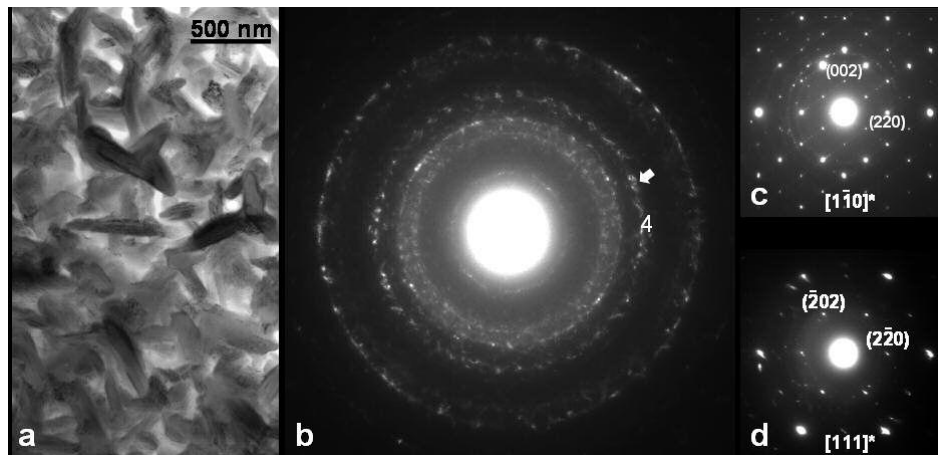


Fig. 10: (a), Bright field image of needle-like grains on some areas of the alloy oxidized at 900°C for 190 min. Electron diffraction ring pattern in (b), and electron diffraction patterns in (c) and (d) taken from individual needles identified the oxide to be γ - Al_2O_3 .

To verify the presence of α -Al₂O₃ in the initial scales formed on Fe₃Al, PL spectroscopy was used. This technique can detect α and θ Al₂O₃ with high sensitivity via the Cr³⁺ emission line which appears at 14,420 and 14460 cm⁻¹, respectively, in the two phases [17,18]. Data from Fe-28Al-5Cr oxidized at 900°C and Ni-50Al oxidized at 1000°C is shown in Fig. 11. The positions of the unstrained α -Al₂O₃ and θ -Al₂O₃ peaks are marked by dashed lines. The results presented in Fig. 11 give a clear indication that α -Al₂O₃ is present in all the early scales formed at 900°C on Fe-28Al-5Cr. The peak intensity increased with time, which can be caused by scale growth (thickening), diffusion of more Cr into the scale, and/or an increase of the α phase in the scale. The behavior is very different from that seen on a NiAl alloy, oxidized at even higher temperatures, 1000°C, where only θ -Al₂O₃ but not α -Al₂O₃ was detected. Although TEM studies showed the presence of θ -Al₂O₃ in the early scales formed on the Fe-28Al-5Cr alloy, this phase was not seen in PL; evidently the detection limit of this phase is lower than for the alpha phase. We note that a longer integration time was needed for the θ -Al₂O₃ signal on NiAl whose Al₂O₃ scale consisted mainly of the theta form and was much thicker than that on the Fe-28Al-5Cr alloy (the concentration of the Cr impurity in this scale formed on NiAl may also have been lower). A Fe-28at%Al alloy without any Cr, but oxidized under the same conditions, i.e., 900°C for 4.5, 30 and 190 minutes, was also tested to evaluate the role of Cr. In all of these samples, α -Al₂O₃ was again found; an example from the 30 min specimen is included in Fig. 11. However, the peak intensities compared with that from the Cr-containing Fe₃Al oxidized under the same condition were significantly lower; we attribute that to a lower concentration of Cr in the scale.

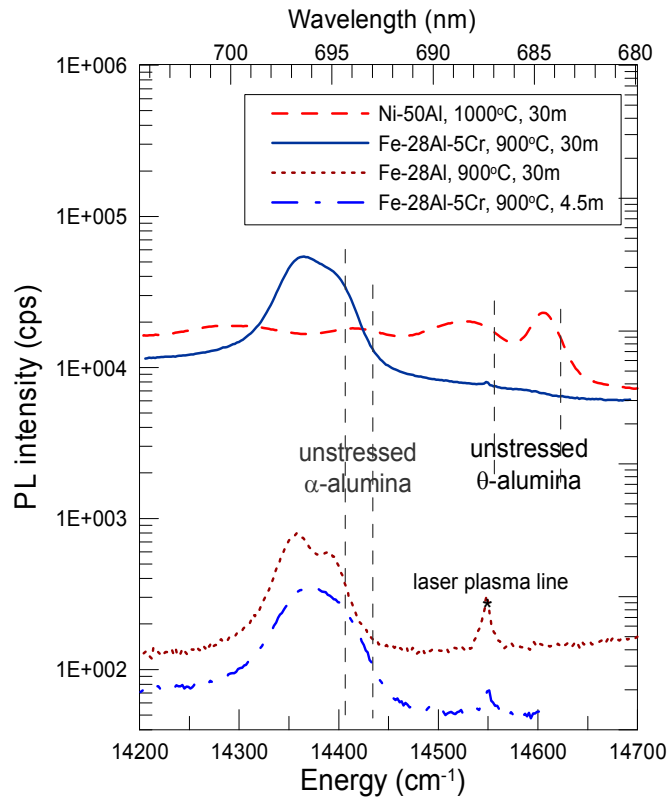


Fig. 11: Luminescent spectroscopy of Al_2O_3 scales formed on Fe-28Al-5Cr (at%) alloys at 900°C after 4.5 and 30 min oxidation. Dashed lines mark peak positions of the unstrained α - and θ - Al_2O_3 . Results for scales formed on Ni-50Al and Fe-28Al (at%) alloys are included for comparison. Signal collection time was 10 sec/step for all the Fe-based alloys, but 25 sec/step for the NiAl.

IV. DISCUSSION

Unlike Ni_3Al , where NiO and Ni-Al spinels were often found at the outer scale surface [7-9], the Fe_3Al alloy studied here did not develop noticeable amounts of Fe-containing oxides above a slow growing Al_2O_3 layer, but only had Fe in solution within the outer portion of a complete Al_2O_3 scale. Fe_2O_3 may have developed during specimen heat-up, as indicated by Raman spectroscopy in an earlier work with slow heating [11], but even there, the Fe_2O_3 signal disappeared shortly before 900°C. TEM studies carried out in this work did not detect any Fe_2O_3 or Cr_2O_3 . Although the current alloy contains 5at%Cr, its presence should not contribute much to the overall scale composition, because Fe-28Al

alloy, without any Cr addition, has also been found by EDS/SEM and X-ray diffraction [16,19] to develop a protective Al_2O_3 layer without the presence of any Fe-containing oxides. The fact that Fe-based aluminide forms Al_2O_3 much faster than its Ni-based counter part is believed to be due to relatively faster diffusion rates of Al in the Fe-based alloy. At 1000°C , the ratio of Al and Fe diffusivity, $D_{\text{Al}}/D_{\text{Fe}}$, in Fe-Al containing 26-50at% Al is 1.4-1.5 [20]. The level, however, is about 5 times lower in nickel aluminide, where $D_{\text{Al}}/D_{\text{Ni}}$ equals to only 0.2-0.3 in Ni_3Al [21]. The faster Al diffusion in iron aluminide can facilitate selective oxidation of the thermodynamically more stable oxide, in this case, Al_2O_3 .

Before oxidation, a room temperature, or native, oxide thin film exists on the alloy surface, as observed by AES depth profile, similar to those shown in Fig. 1. This layer is only several nanometers in thickness and consists of all the alloying elements, similar to that reported for a Fe-20Cr-10Al alloy [22]. During heating, crystallization of the native oxide must occur, and, according to the AES depth profile seen in Fig. 1 on the 4.5 min sample, there is also some Fe oxide growth and the development and extensive growth of an Al_2O_3 layer. Unlike Ni-50Al, which forms an initial surface $\gamma\text{-Al}_2\text{O}_3$ layer that is epitaxially oriented with the substrate [2,4], the Al_2O_3 that forms on this Fe_3Al alloy is a mixture of θ , γ as well as $\alpha\text{-Al}_2\text{O}_3$. There is only textured relationships with the substrate along three, 120° -apart directions, where the $\theta[\bar{1}01]$ and the $\gamma[111]$ are parallel to the substrate $[001]$ direction, with an in-plane rotation of up to 22° , indicating the presence of a non-coherent interface between the initially formed oxide and the substrate. This again, is different from that reported for the Ni-50Al, which forms a coherent $\gamma\text{-Al}_2\text{O}_3/\text{NiAl}$ interface [4].

The presence of the rod-shaped bands mixed in an Al_2O_3 oxide layer has rarely been observed on other alloys, although similar phenomenon was reported in scales formed on NiCrAl [23]. The fact that these bands disappear with oxidation time indicates that they are formed during the initial stage of oxidation. When NiAl is oxidized under low P_{O_2} with doses of oxygen, rod-shaped oxides are formed along the substrate $[001]$ direction, leaving unoxidized regions in between [24,25,26]. The preferential growth direction of

these rods on the alloy surface is a result of strain minimization. When an initial amorphous Al_2O_3 layer exists on the alloy surface prior to heating, the rods are nucleated by the crystallization of this layer at intermediate temperatures [24]. Similar phenomenon may occur on the Fe_3Al studied here. It is likely that a preferential growth direction exists within the very first Al_2O_3 crystals (whether nucleated or crystallized or both). These textured bands grow laterally along three, 120° -apart directions. In between these bands are randomly oriented Al_2O_3 grains of θ , γ as well as α alumina. The textured bands consist mainly of θ and γ - Al_2O_3 , where the two phases intergrown with a fixed orientation relationship. With time, the oxide film thickens and epitaxy is lost, probably due to higher strain levels in the film, and the number density of these bands decrease.

The first-formed Al_2O_3 phases on all nickel aluminides are either the θ , γ form or a mixture of the two [2-9]. α - Al_2O_3 only nucleates later mainly as a result of alumina phase transformation [27,28,29]. However, in this Cr-containing Fe_3Al alloy, α - Al_2O_3 was found at the very early stage, even when the specimen was being heated. The behavior is similar to that observed by Andoh et al [30] on a FeCrAl alloy (about 18wt%Cr and 3-4wt%Al). Cr has been proposed to accelerate α - Al_2O_3 formation where its oxide particles act as nuclei for the θ to α -alumina phase transformation [31]. Although the present Fe_3Al alloy contains 5at%Cr, there is no experimental evidence showing that the Cr is responsible in enhancing α - Al_2O_3 nucleation. However, since the alloy has been found to form a small amount of Fe_2O_3 during heating, as previously observed by Raman spectroscopy [11], and that current TEM and AES results have found Fe in solution within the outer portion of the Al_2O_3 scale, the initially formed Fe_2O_3 , being isomorphous with α - Al_2O_3 , may also be able to enhance α - Al_2O_3 nucleation. This conclusion is confirmed by the fact that α - Al_2O_3 also forms on Fe-28Al during the early stages of oxidation (Fig. 11), where there is no Cr in the alloy. These results are in agreement with the earlier proposals [12,11] that the initially formed Fe_2O_3 act as templates to help nucleate α - Al_2O_3 . Because of this reason, no α phase was detected in the initial scales formed on NiAl alloys [2-9].

From the TEM results and the above discussions, we can derive the growth mechanism of the Al_2O_3 scale on our Fe_3Al -based alloy at 900-1000°C as follows.

Initially, textured θ/γ bands were formed along preferred orientations, with α and θ alumina growing between these bands; the $\alpha\text{-Al}_2\text{O}_3$ formed early due to the presence of Fe_2O_3 in the native and initial oxide film acting as its nucleation sites. At this stage, the slow growing α -grains have not fully developed into a complete layer, therefore, the scale thickened through outgrowth of the γ/θ layer, and the newly formed top layer was usually porous. Transformation of the abundant θ and γ grains in the initial scale into $\alpha\text{-Al}_2\text{O}_3$ took place at the scale/alloy interface, giving rise to large, new alpha grains, just as in the case of NiAl. However, due to the presence of $\alpha\text{-Al}_2\text{O}_3$ in the initial γ/θ layer, the development of this $\alpha\text{-Al}_2\text{O}_3$ layer at the interface was much faster on the Fe-based alloy. Eventually, growth of the oxide scale was dominated by the α -grain layer which had fully covered the substrate surface. After longer oxidation times, the oxide film was composed of mainly α - alumina grains with a top layer containing $\gamma/\theta\text{-Al}_2\text{O}_3$. Transformation of the residual γ/θ -grains into $\alpha\text{-Al}_2\text{O}_3$ will eventually be completed at the elevated oxidation temperatures.

V. CONCLUDING REMARKS

Formation, structure, and phase development in Al_2O_3 scales on a Fe_3Al -based Fe-28Al-5Cr (at %) alloy after different oxidation times at elevated temperatures were studied using Auger electron spectroscopy, TEM, and luminescent spectroscopy. The results and conclusions are summarized as following:

- (1) θ -, γ -, as well as $\alpha\text{-Al}_2\text{O}_3$ polymorphs were detected in the initial scales, even during heating, with small amounts of Fe in solution near the scale outer region. The oxide films at this time were single layered. With extended oxidation, at an oxide thickness of about $0.5\ \mu\text{m}$, large $\alpha\text{-Al}_2\text{O}_3$ grains nucleated at the scale/alloy interface and the oxide became double layered with the inner layer being $\alpha\text{-Al}_2\text{O}_3$, and the outer layer being an mixture of γ and $\theta\text{-Al}_2\text{O}_3$. At some surface locations, the $\gamma\text{-Al}_2\text{O}_3$ developed into needle shaped grains.

- (2) The initial scale contained band-like structures that extended along three directions with a 120° angle between them. Textured θ and γ grains were the main components in these bands, and fine grained α - Al_2O_3 mixed with randomly oriented θ and γ - Al_2O_3 phases existed between them. A likely orientation relationships between the textured bands and the substrate are $[001]_{\text{Fe}_3\text{Al}}//[\bar{1}01]_{\theta\text{-Al}_2\text{O}_3}//[111]_{\gamma\text{-Al}_2\text{O}_3}$, with an in-plane rotation angle between 0 and 22° . The amount of these oriented grains decreased with oxidation time.
- (3) α - Al_2O_3 was also detected in the early scale grown on Fe-28Al without the 5%Cr addition, although in smaller quantities. This phenomenon is different from that reported for NiAl, demonstrating that Fe_2O_3 , which were initially present on the alloy surface, can act as templates for α - Al_2O_3 nucleation, giving rise to a much faster θ/γ to α transformation than in the NiAl case.
- (4) Alumina scale development on Fe_3Al is similar to that on β -NiAl where a layer of oxide consisting mainly of transition Al_2O_3 first forms, followed by the nucleation and growth of an α - Al_2O_3 layer at the scale/alloy interface. However, the behavior is different from that of its counter part, Ni_3Al , where extensive Ni oxidation takes place. The difference is believed to be associated with faster diffusion rates of Al relative to Fe in Fe_3Al than of Al compared to Ni in Ni_3Al .

ACKNOWLEDGMENTS

The authors would like to thank Dr. Peter Tortorelli for supplying the alloy. This research was sponsored by the U. S. Department of Energy under contract No. DE-AC03-76SF0098. The work was made possible through the use of the National Center for Electron Microscopy facility at the Lawrence Berkeley National Laboratory.

REFERENCES

1. M. P. Brady, B. A. Pint, P. F. Tortorelli, I. G. Wright and R. J. Hanrahan, Jr.: High temperature oxidation and corrosion of intermetallics, in *Corrosion and Environmental Degradation*, pp. 232-325, edited by M. Schutze (Materials Science and Technology, V. 19, Wiley-VCH, New York, 2000).
2. J. Doychak, J. L. Smialek and T. E. Mitchell: Transient oxidation of single-crystal β -NiAl. *Met. Trans. A* **20A**, 499 (1989).
3. G. C. Rybicki and J. L. Smialek: Effect of the θ - α -Al₂O₃ transformation on the oxidation behavior of β -NiAl+Zr. *Oxid. Metals* **31**, 275 (1989).
4. J. C. Yang, K. Nadarzynski, E. Schumann and M. Rühle: Electron microscopy studies of NiAl/ γ -Al₂O₃ interface. *Scripta Met* **33**, 1043 (1995).
5. J. C. Yang, E. Schumann, I. Levin and M. Rühle: Transient oxidation of NiAl. *Acta Metall* **46**, 2195 (1998).
6. J. L. Smialek, J. Doychak and D. J. Gaydosch: Oxidation behavior of FeAl + Hf, Zr, B. *Oxid. Metals* **34**, 259 (1990).
7. J. D. Kuenzly and D. L. Douglass: *Oxid. Metals* **8**, 139 (1974).
8. J. Doychak and M. Rühle: TEM studies of oxidized NiAl and Ni₃Al cross sections. *Oxid. Metals* **31**, 431 (1989).
9. E. Schumann and M. Rühle: Microstructural observation on the oxidation of γ' -Ni₃Al at high oxygen partial pressure. *Acta metall. mater.* **42**, 1481 (1994).
10. See for example, K. B. Alexander, K. Prussner, P. Y. Hou and P. F. Tortorelli: Microstructure of alumina scales and coatings on zirconium-containing iron aluminide alloys. *Microscopy of Oxidation 3*, ed. S. B. Newcomb and J. A. Little, pp. 246-264, The Institute of Metals, 1997.
11. D. Renusch, M. Grimsditch, I. Koshelev, B. W. Veal, and P. Y. Hou: Strain determination in thermally grown alumina scales using fluorescence spectroscopy. *Oxid. Metals* **48**, 471 (1997).
12. W. C. Hagel: The oxidation of iron, nickel and cobalt-based alloys containing aluminum. *Corrosion*, **21**, 316-326 (1965).
13. P. Y. Hou: Sulfur segregation to growing Al₂O₃/alloy interfaces. *J. Mater. Sci. Lett.* **19**, 577 (2000).
14. C. G. McKamey, P. J. Mazdiaz, G. M. Goodwin and T. Zacharia: Effects of alloying additions on the microstructures, mechanical properties and weldability of Fe₃Al-based alloys, in *Materials Science & Engineering A-Structural Materials Properties Microstructure & Processing*, vol.A174, no.1, Jan. 1994, p.59.
15. M. Tinker and P.A. Labun: Transmission electron microscopy of transverse sections through oxide scales on metals. *Oxid. Metals*, **18**, 27-40 (1982).
16. Z. G. Yang and P. Y. Hou: Wrinkling behavior of alumina scale formed during isothermal oxidation of FeAl binary alloys. *Mater. Sci. Eng. A* **391**, 1 (2005).

17. Q. Ma, M. C. Shaw, M. Y. He, B. J. Dalgleish, D. R. Clarke and A. G. Evans: Stress redistribution in ceramic/metal multilayers containing cracks, in *Acta Metallurgica et Materialia*, vol.43, no.6, June 1995, p.2137.
18. Qingzhe Wen, D. M. Lipkin and D. R. Clarke: Luminescence characterization of chromium-containing theta-alumina. *J. Am. Ceram. Soc.* **81**, 3345 (1998).
19. P. Y. Hou, A. P. Paulikas and B. W. Veal: Growth strains and stress relaxation in alumina scales during high temperature oxidation. *Mater. Sci. Forum* **461-464**, 671 (2004).
20. Y. H. Sohn and M. A. Dayananda: Interdiffusion, intrinsic diffusion and vacancy wind effect in Fe-Al alloys at 1000°C. *Scripta Mater.* **40**, 79 (1999).
21. T. Ikeda, A. Almazouzi, H. Numakura, M. Koiwal, W. Sprengel and H. Nakajima: Single-phase interdiffusion in Ni₃Al. *Acta Materialia*, **46**, 5369-76 (1998).
22. P. Y. Hou, X. F. Zhang and R. M. Cannon: Impurity distribution in Al₂O₃ formed on an FeCrAl alloy. *Scripta Mater* **51**, 45 (2004).
23. J. L. Smialek and R. Gibala: Structure of Transient Oxides Formed on NiCrAl Alloys. *Metall. Trans. A*, **14A**, 2143-2161 (1983).
24. K. F. McCarty: Imaging the crystallization and growth of oxide domains on the NiAl(110) surface. *Surf. Sci.* **474**, L165, (2001).
25. N. Fremy, V. Maurice and P. Marcus: Initial stages of growth of alumina on NiAl(001) at 1025 K. *J. Am. Ceram. Soc.* **86**, 669 (2003).
26. J. P. Pierce and K. F. McCarty: Self-assembly and dynamics of oxide nanorods on NiAl(110). *Phys. Rev. B*, **71**, 125428 (2005).
27. D.M. Lipkin, H. Schaffer, F. Adar, and D.R. Clarke: Lateral growth kinetics of α -alumina accompanying the formation of a protective scale on (111) NiAl during oxidation at 1100°C. *Appl. Phys. Lett.* **70**, 2550 (1997).
28. V.K. Tolpygo, and D.R. Clarke: Microstructural study of the theta-alpha transformation in alumina scales. *Mater. High Temp.* **17**, 59, (2000).
29. P. Y. Hou, A. P. Paulikas and B. W. Veal: Stress development and relaxation in Al₂O₃ during early stage oxidation of β -NiAl. to be published in *Mater. High Temp.*
30. A. Andoh, S. Taniguchi, and T. Shibata: TEM observation of phase transformations of alumina scales formed on Al-Deposited Fe-Cr-Al foils. *Mater. Sci. Forum* **369-372**, 303, (2001).
31. R. Klumpes, C. H. M. Maree, E. Schramm and J. H. W. de Wit: The influence of chromium on the oxidation of β -NiAl at 1000°C. *Materials & Corrosion-Werkstoffe und Korrosion* **47**, 619 (1996).

FIGURE CAPTIONS

Fig. 1: Auger electron spectroscopy depth profiles of scales formed on a Fe₃Al-based Fe-28Al-5Cr alloy after (a), 3 min and (b), 10 min in a 1000°C furnace.

Fig. 2: (a), Cross-sectional morphology of Al₂O₃ scale oxidized on a Fe₃Al alloy at 900°C for 4.5 min. The glue layer was applied during TEM sample preparation. (b), EDS line scan across the thickness of Al₂O₃ scale.

Fig. 3: High-resolution electron micrograph showing two nanoscale grains in the cross-sectional Al₂O₃ scale oxidized at 900°C for 4.5 min. Lattice fringes within grains are recognized.

Fig. 4: Cross-sectional TEM images of an alloy oxidized at 1000°C for 10 min. (a) α-Al₂O₃ grains nucleated at the scale/alloy interface as indicated by arrows. Small voids are seen in the scale between the alpha and transition alumina, and (b) large voids are sometimes detected at the scale/alloy interface.

Fig. 5: (a), Bright-field plan-view TEM image taken from the Al₂O₃ scale oxidized on a Fe₃Al alloy at 900°C for 4.5 min. Corresponding electron diffraction ring pattern is inserted, in which strong reflection loci used for dark-field imaging are circled and marked with 1, 2, and 3. (b), (c), (d), Dark-field images using diffraction spots 1, 2, and 3, respectively, marked in the inset of (a).

Fig. 6: (a), Plan-view morphology of Al₂O₃ scale oxidized on a Fe₃Al alloy at 900°C for 35 min. Arrows indicate dark-contrast bands which are along three directions as marked by lines. (b), Electron diffraction ring pattern taken with a 4.4 μm diameter selected-area aperture. d-spacing values and the Al₂O₃ polymorphs corresponding to the rings marked by 1, 2, 3, and 4, respectively, are listed in an inserted table. Arrows indicate strongly excited diffraction loci on a diffraction ring.

Fig. 7: (a), Plan-view morphology of the Al₂O₃ scale oxidized on a Fe₃Al alloy at 900°C for 190 min. The band structure observed in the 4.5 and 35 min oxidation films

disappeared. (b), Corresponding electron diffraction ring pattern taken from a 4.4 μm diameter area.

Fig. 8: (a), Selected-area electron diffraction pattern taken from Al_2O_3 scale oxidized on a Fe_3Al alloy at 900°C for 4.5 min. A 1.8 μm diameter selected-area aperture was used. Strongly excited diffraction loci with a 3- or 6-fold symmetric arrangement can be seen. (b), Electron diffraction pattern taken from a 0.2 μm diameter area within the single band as shown in Fig. 5a. Diffraction spots from θ - and γ - Al_2O_3 phases are connected with solid and dashed lines, respectively.

Fig. 9: (a), Electron diffraction pattern taken from Al_2O_3 scale oxidized on a Fe_3Al alloy at 900°C for 35 min. Diffraction spots from Fe_3Al substrate (denoted as FA) projected along the $[001]$ direction are indexed. Superimposed diffraction rings from Al_2O_3 scale are seen. Strongly excited, 3- or 6-fold symmetric loci are indicated by arrows. (b), Simulated Fe_3Al $[001]$ electron diffraction pattern is superimposed on a simulated θ - Al_2O_3 $[\bar{1} 01]$ diffraction pattern. A dashed circle marks the $\theta(111)$ ring which matches the ring marked by the dashed circle in (a).

Fig. 10: (a), Bright field image of needle-like grains on some areas of the alloy oxidized at 900°C for 190 min. Electron diffraction ring pattern in (b), and electron diffraction patterns in (c) and (d) taken from individual needles identified the oxide to be γ - Al_2O_3 .

Fig. 11: Luminescent spectroscopy of Al_2O_3 scales formed on Fe-28Al-5Cr (at%) alloys at 900°C after 4.5 and 30 min oxidation. Dashed lines mark peak positions of the unstrained α - and θ - Al_2O_3 . Results for scales formed on Ni-50Al and Fe-28Al (at%) alloys are included for comparison. Signal collection time was 10 sec/step for all the Fe-based alloys, but 25 sec/step for the NiAl.